PHOTOSYNTHETICA
International Journal for Photosynthesis Research

DOI 10.32615/ps.2024.012 PHOTOSYNTHETICA 62 (2): 168-179, 2024

Selenite foliar application increased the accumulation of medicinal components in *Paeonia ostii* by promoting antioxidant capacity, reducing oxidative stress, and improving photosynthetic capacity

L.X. ZHANG[*,+,†], Q.S. CHANG[**,†], Y.L. HE[*], X.L. ZHAO[*], W. LIU[*], Q. GUO[*], K. CHEN[*], and X.G. HOU[*,+]

College of Agriculture, Henan University of Science and Technology, 471003 Luoyang, China[*]
College of Horticulture and Plant Protection, Henan University of Science and Technology, 471003 Luoyang, China[**]

Abstract

The effects of selenite (0, 15, 30, 45 mg L^{-1}) on physiological characteristics and medicinal components of *Paeonia ostii* were analyzed. The results showed that selenite application promoted the activity of superoxide dismutase and the contents of soluble sugar, proline, carotenoids, total flavonoids, and total polyphenols, and decreased the contents of reactive oxygen species, relative electrical conductivity, and malondialdehyde. In addition, selenite also increased chlorophyll content, improved electron transfer ability, PSI and PSII performance, and the coordination between PSI and PSII, which significantly improved photosynthetic capacity. Moreover, selenite treatment also greatly increased the contents of gallic acid, catechin, albiflorin, paeoniflorin, benzoic acid, and paeonol in Moutan cortex radicis (MCR). These results showed that selenite effectively protected the photosynthetic apparatus from photooxidative damage by enhancing antioxidant capacity, improving photosynthetic capacity, and increasing the content of the medicinal compounds in MCR.

Keywords: chlorophyll fluorescence; *Paeonia ostii*; photosynthesis; secondary metabolites; selenite.

Highlights

- Selenite improved the antioxidant system and reduced the oxidative stress in *Paeonia ostii*
- Selenite improved the performance of PSI and PSII, thereby promoting the increase of P_N
- Selenite enhanced medicinal components in Moutan cortex radicis of *Paeonia ostii*

Received 18 October 2023
Accepted 6 February 2024
Published online 21 March 2024

[+]Corresponding authors
e-mail: hkdzlx@126.com (L.X. Zhang)
hkdhxg@haust.edu.cn (X.G. Hou)

Abbreviations: ABS/CS_m – the absorbed energy flux per cross-section; ABS/RC – the absorption flux per reaction center; Car – carotenoid; Chl – chlorophyll; C_i – intercellular carbon dioxide concentration; DI_0/CS_m – the dissipated energy flux per cross-section; DI_0/RC – the dissipated energy flux per reaction center; E – transpiration rate; ET_0/CS_m – the electron transport flux per cross-section; ET_0/RC – the electron transport flux per reaction center; ETR – the rate of electron transfer; F_v/F_m – the maximum photochemical efficiency of PSII under dark adaptation; F_v'/F_m' – the efficiency of excitation capture of open PSII center; g_s – stomatal conductance; M_0 – the initial slope of the relative variable fluorescence of the relative rate at which Q_A is reduced; MCR – Moutan cortex radicis; MDA – malondialdehyde; PI_{abs} – the performance index on absorption basis; P_N – the net photosynthetic rate; RC/CS_m – the density of RCs per excited cross-section; REC – the relative electrical conductivity; ROS – reactive oxygen species; SOD – superoxide dismutase; TR_0/CS_m – the trapped energy flux per cross-section; TR_0/RC – the trapped energy flux per reaction center; V_J – the relative variable fluorescence intensity at the J step; W_K – the normalized relative variable fluorescence; $\Delta I/I_0$ – the maximum redox activity of PSI; φE_0 – the quantum yield for electron transport; $\Phi_{PSI/PSII}$ – the coordination between PSI and PSII; Φ_{PSII} – the actual photochemical efficiency of PSII.

Acknowledgements: This work was supported by the Application Research Joint Fund Project of Henan Province (222103810057), the Key Technology Research and Development Program of Henan Province (212102110475), and the Project for the Technical System of Traditional Chinese Medicinal Material Industry in Henan Province (YuCaiKe [2022] No. 24).

[†]These authors contributed equally to this work.

Conflict of interest: The authors declare that they have no conflict of interest.

Introduction

Tree peony (*Paeonia* sect. Moutan) is a famous traditional flower originating in China, which has not only ornamental value but also important medicinal value, and *Paeonia ostii* 'Fengdan' is one of the most representative cultivated varieties (Sun *et al*. 2021). Moutan cortex radicis (MCR) is the dry root bark of perennial tree peony root after removing the internal core, and it is rich in phenols, flavonoids, and terpenoids, such as paeonol, paeoniflorin, gallic acid, catechin, albiflorin, benzoic acid, *etc*. Studies have shown that these phenolic acids and flavonoids have antioxidant properties (Wang *et al*. 2019, Jucá *et al*. 2020), which are an important part of plant nonenzymatic antioxidants and another line of defense against reactive oxygen species (ROS) (Lanza and Reis 2021). MCR has a wide range of clinical applications, such as the functions of promoting blood circulation, cooling blood, clearing heat, and removing blood stasis, and is broadly used in traditional Chinese medicine for thousands of years (Wang *et al*. 2019). In China, MCR is used as an important crude drug in many traditional Chinese patent medicines to treat various diseases such as cardiovascular, extravasated blood, and tumors (Wang *et al*. 2017). Therefore, increasing the active components in MCR is of great importance to improve the quality of medicinal materials and the therapeutic effect on related diseases.

Studies have shown that the application of exogenous sodium selenite can regulate growth and development, as well as the synthesis and accumulation of secondary metabolites, thereby improving the intrinsic quality of crops (Li *et al*. 2022a). Selenium is an essential trace element for humans and plants, which is the constituent and active center of glutathione peroxidase (GSH-Px) (Puccinelli *et al*. 2020). Selenium is mainly absorbed by plants in the form of selenite (IV), selenate (VI), and organic selenium compounds; selenite and selenate are the two most widely used forms in selenium fertilizer applications. In plants, selenium in organic form is safer and more effective than selenium in inorganic form for human beings and animals (Rider *et al*. 2010, Kalaei *et al*. 2022). It is found that foliar application of selenite can promote the biosynthesis of organic selenium (IV) more effectively compared to selenate (VI) in onions, carrots (Kápolna *et al*. 2012), and corn (Longchamp *et al*. 2015). This view was also proved in wheat; wheat particles sprayed with selenite have a higher percentage of organic selenium than those sprayed with sodium selenate (Wang *et al*. 2020a). Therefore, the foliar application of sodium selenite is a popular selenium application method.

Selenium has a wide range of antioxidant capacities, which can increase the activities of GSH-Px, superoxide dismutase (SOD), peroxidase (POD), and other enzymes, thus increasing the scavenging capacity of ROS (Lanza and Reis 2021). The application of sodium selenite further increased the activities of antioxidant enzymes and alleviated the negative effects of cadmium stress in *Solanum lycopersicum* seedlings (Alyemeni *et al*. 2018). Quinoa plants showed a significant increase in SOD, catalase (CAT), POD, ascorbate peroxidase (APX), and glutathione reductase (GR) activities, and a decrease in malondialdehyde (MDA) and hydrogen peroxide (H_2O_2) at low concentrations of sodium selenite and sodium selenate (Khalofah *et al.* 2021). Selenium can also promote the increase of nonenzymatic active substances, soluble protein, soluble sugar, and proline content. In *Brassica pekinensis*, foliar spraying of sodium selenite significantly increased vitamin C, proline, protein, and sugar content (Liu *et al.* 2020). Similarly, spraying 10 mg L^{-1} of sodium selenite significantly increased soluble protein and soluble sugar content in mustard (Li *et al.* 2023). In addition, selenium can regulate the synthesis of amino acids and proteins, as well as N-secondary compounds, such as phenolics and flavonoids with free radical scavenging activities (Malagoli *et al*. 2015). In mustard, the concentration of 10 mg L^{-1} Na_2SeO_3 significantly increased the contents of flavonoids, total phenols, vitamin C, and anthocyanins compared with the control (Li *et al.* 2023). Foliar spraying of sodium selenite under drought stress significantly increased total phenolic content, anthocyanins, and flavonoids in camelina and canola (Ahmad *et al.* 2021).

Photosynthesis consists of three important steps: primary reaction, including absorption, transfer and conversion of light energy, electron transport and photophosphorylation, and carbon assimilation step (Cruz and Avenson 2021). The normal operation of photosynthesis depends on the coordination of photosynthetic pigment, photosynthetic electron transport chain and PSI and PSII (Zhang *et al*. 2023). Recent studies showed that selenite played an effective role in promoting functionality of the photosynthetic apparatus. In *Billbergia zebrina*, selenite application improved the potential capacity of energy conservation in the photosynthetic apparatus and the electron transport dynamics between the intersystem and PSI (Souza *et al*. 2019). In *Medicago sativa*, selenite treatment greatly increased the pigment contents, and the maximal quantum yield of PSII photochemistry (F_v/F_m) (Wang *et al*. 2022).

To the best of our knowledge, the literature lacks information on exogenous selenite application on the physiology and secondary metabolism accumulation, especially, its effects on PSI and PSII in tree peony. Therefore, it is necessary to study the effects of selenite on antioxidant activity, pigment content, photosynthetic parameters, structure and function of PSII and PSI, and medicinal component accumulation of tree peony. The aim of this study was to investigate whether there was a positive effect of selenite on *P. ostii* plants and whether the contents of beneficial phytochemicals (such as paeonol and paeoniflorin) increased in MCR.

Materials and methods

Plant material and experimental conditions: Pot experiments were conducted in the experimental farm of Henan University of Science and Technology, Henan Province, China. In October 2021, healthy and uniform five-year-old *P. ostii* cv. 'Fengdan' seedlings were planted in plastic pots filled with 12 kg of mixed nutrient soil

(V_{soil}:V_{sand}:$V_{organic\ matter}$ = 3:1:1), and then cultivated outside. The flower buds of *P. ostii* were removed in March 2022. Since 30 March, all seedlings were sprayed with 0.2% KH_2PO_4 solution every 20 d for three times. A completely randomized design was used with 12 replications (pots) for each treatment. The seedlings were sprayed with sodium selenite solution (0, 15, 30, 45 mg L^{-1}) for three times on 10 April, 30 April, and 20 May 2022, respectively. Using *Tween-80* (0.1%) as surfactant, selenite solution was sprayed on the adaxial and abaxial surfaces. The pots were covered with plastic film before spraying in case the selenite solution was introduced into the soil. All pots were watered normally to avoid drought stress. After 10 d of treatment, the physiological parameters were determined. MCR was harvested to determine the content of secondary metabolites in October 2022.

Superoxide dismutase activity: SOD (EC 1.15.1.1) activity was evaluated using the photochemical nitroblue tetrazolium (NBT) method described by Li *et al*. (2018). Fresh leaves (0.50 g) were homogenized in 50 mM phosphate buffered-saline (PBS, pH 7.8), and then centrifuged at 4,000 rpm at 4°C for 20 min to obtain the supernatant. Supernatant (0.2 mL) was mixed with 50 mM PBS, 100 mM ethylenediamine tetraacetic acid disodium salt, 130 mM methionine, 0.75 mM NBT, and 20 μM riboflavin to form 3 mL of the reaction solution. The absorbance of the mixture at 560 nm was measured by a spectrophotometer (*752N*, *INESA*, China).

Soluble protein, soluble sugar, and proline content: The content of soluble protein was determined as described by Wang *et al*. (2015). First, 0.25 g of fresh leaves were homogenized in 10 mL of distilled water, then the supernatant was obtained after centrifugation at 3,000 rpm for 10 min at 4°C. Finally, the supernatant was mixed with 5.0 mL of *Coomassie Brilliant Blue G250* for 2 min, then the soluble protein content was calculated using the absorbance at 595 nm. The soluble protein content was expressed as mg g^{-1}.

The content of soluble sugar was determined as proposed by Dong *et al*. (2019). Fresh leaves (0.10 g) were placed in a test tube filled with distilled water, and extracted twice in boiling water for 30 min. Then, the extract (0.5 mL) was mixed with deionized water (1.5 mL), anthrone ethyl acetate reagent (0.5 mL), and concentrated sulfuric acid (5 mL), and boiled for 1 min. The absorbance of the extract at 630 nm was measured by a spectrophotometer (*752N*, *INESA*, China). The soluble sugar content was expressed as mg g^{-1}.

The proline content was determined according to Bates *et al*. (1973). Fresh leaves (0.20 g) were placed in a test tube, and 3% sulfosalicylic acid aqueous solution was added and extracted in boiling water for 10 min. Then 2 mL of supernatant was mixed with equal volumes of acetic acid and acidic ninhydrin and boiled for 0.5 h. Then toluene was added and fully shaken to obtain an extract. The absorbance was measured at 520 nm using a spectrophotometer (*752N*, *INESA*, China). The proline content was expressed as μg g^{-1}.

Relative electrical conductivity and malondialdehyde content: The relative electrical conductivity (REC) was assessed as previously described (Zhang *et al*. 2021). Fresh leaves (0.10 g) were rinsed and cut into thin strips, then mixed with 6 mL of distilled water, and incubated at room temperature for 24 h. The initial electrical conductivity (EC1) was measured with an electrical conductivity meter (*DDS-11A*, Shanghai, China). Then leaf samples were boiled for 0.5 h, and the electrical conductivity was determined again (EC2) after cooling, REC was calculated as the percentage ratio of EC1/EC2 × 100%.

MDA was measured as described previously (Cai *et al*. 2019). Fresh leaves (0.25 g) were triturated using 5 mL of 5% (w/v) trichloroacetic acid and centrifuged at 10,000 rpm for 10 min. The supernatant (2 mL) was mixed with 2 mL (0.67%, w/v) thiobarbituric acid, then boiled for 30 min, cooled and centrifuged at 10,000 rpm for 10 min again, and then the absorbance was measured at 450, 532, and 600 nm. The MDA content was expressed as nmol g^{-1}.

Determination of H_2O_2 and superoxide radical ($O_2^{\bullet-}$): H_2O_2 content was determined according to Cheeseman (2006). Fresh leaf samples (0.60 g) were ground in 1% trichloroacetic acid (5 mL) and centrifuged for 10 min at 4°C, then the supernatant (0.70 mL) was added to 10 mM PBS (0.7 mL, pH 7.0) and 1 M iodide potassium (1.4 mL). After 20 min in the dark, the absorbance of the supernatant at 390 nm was measured. The content of H_2O_2 was expressed as μmol g^{-1}.

$O_2^{\bullet-}$ content was measured by the method of Zhang *et al.* (2021). Fresh leaf samples (1.0 g) were homogenized in 5 mL of PBS (65 mM, pH 7.8), filtered, and centrifuged for 10 min at 10,000 rpm. After that, the extract (2 mL) was mixed with 65 mM PBS (1.5 mL, pH 7.8) and 10 mM hydroxylamine hydrochloride (0.5 mL), and the mixture was incubated at 25°C for 20 min. The final mixture (2 mL) was transferred to a test tube containing 17 mM p-sulfanilic acid (2 mL) and 7 mM α-naphthylamine (2 mL), incubated again at 30°C for 30 min. Finally, the $O_2^{\bullet-}$ content was quantified spectrophotometrically at 530 nm. The content of $O_2^{\bullet-}$ was expressed as μg g^{-1}.

Photosynthetic pigments and gas-exchange parameters: Pigment contents of chlorophyll (Chl) *a*, Chl *b*, and carotenoids (Car) were measured according to the method of Lichtenthaler (1987). Fresh leaves (0.10 g) were extracted with 80% acetone solution for 48 h in the dark. Then the absorbance of the extract was determined at 470, 646, and 663 nm. The pigment contents were expressed as mg g^{-1}.

At 9:00–11:00 h on sunny days, photosynthetic parameters, such as net photosynthetic rate (P_N), intercellular CO_2 concentration (C_i), stomatal conductance (g_s), and transpiration rate (E), were measured using *LI-6400* portable photosynthetic system (*LI-COR*, Lincoln, NE, USA). The detection conditions were as follows: illumination intensity was 1,200 μmol(photon) m^{-2} s^{-1}, leaf chamber temperature was 25°C, CO_2 concentration was 380 μmol mol^{-1}, and the airflow rate was 500 μmol s^{-1}.

Five biological repeats were performed for all treatments, with three leaves selected for each repetition.

Chl fluorescence, the rapid Chl fluorescence induced curve (OJIP), and 820-nm modulation reflection curve: Chl fluorescence was measured using a modulated fluorometer (*MINI-PAM 2000*, *WALZ*, Germany). The initial fluorescence in the light-adapted state (F_0') and maximal fluorescence in the light-adapted state (F_m') were measured by using saturating pulses and far-red light, respectively. The efficiency of excitation capture of open PSII center (F_v'/F_m'), the actual photochemical efficiency of PSII (Φ_{PSII}), and the rate of electron transfer (ETR) were then recorded according to the method of Genty *et al*. (1989).

The OJIP curve and 820-nm modulation reflection curve were simultaneously measured by *M-PEA* (*Hansatech*, Norfolk, UK) (Strasser *et al.* 2010). The leaves were dark-adapted for at least 1 h, then exposed to the saturated red light of 3,000 μmol(photon) m^{-2} s^{-1} to obtain OJIP curve parameters (Appendix 1), the 820-nm modulated reflection curve was measured by exposure to 250 μmol(photon) m^{-2} s^{-1} far-red light. The relative variable fluorescence (V_t) at any time was calculated according to the formula: $V_t = (F_t - F_0)/(F_m - F_0)$ (Li *et al*. 2020). The 820-nm modulation reflection curve was plotted according to the value of MR/MR_0 (MR is the modulation reflection at different time points, and MR_0 is the MR value of far-red light irradiated with 0.7 ms) (Strasser *et al*. 2010). The maximum redox activity of PSI ($\Delta I/I_0$) and the coordination between PSI and PSII ($\Phi_{PSI/PSII}$) were calculated according to the formula: $\Delta I/I_0 = (I_0 - I_m)/I_m$, $\Phi_{PSI/PSII} = (\Delta I/I_0)/\psi_0$ (Zhang *et al*. 2021). At least ten biological repeats were measured for each treatment.

Total flavonoids, total phenolic, and secondary metabolites content: The method proposed by Chen *et al*. (2019) was used to determine the content of total flavonoids. The MCR powder was placed in a conical flask filled with 60% ethanol solution, extracted in a water bath at 70°C for 1.5 h, and centrifuged at 4,000 rpm for 10 min. A volume of 0.25 mL of the above solution was added to 0.3 mL of 5% $NaNO_2$ solution and shaken for 6 min. Then, 0.3 mL of 10% $Al(NO_3)_3$ solution was added to the above mixture, shaken well, and left for 6 min, then 4 mL of NaOH (4%) solution was added, and the absorbance at 510 nm was measured after full shock and left for 10 min at constant volume. The content of total flavonoids was expressed as mg g^{-1}.

The total phenolic content was determined according to the method of Feng *et al*. (2014). MCR (0.2 g) was added to 5 mL of 80% methanol and extracted by ultrasound at 25°C for 5 min, centrifuged at 10,000 rpm for 10 min to obtain supernatant. After that, 5 mL of 80% methanol was added to the precipitation, and the supernatant was combined after repeated extraction for four times. Then, 0.1 mL of extract and 0.4 mL of distilled water were mixed with 2.5 mL of 10% Folin–Ciocalteu's reagent, and then 2 mL of 7.5% Na_2CO_3 solution was added and incubated in the dark at room temperature for 1 h. The absorption value was determined at 765 nm using a spectrophotometer (*752N*, *INESA*, China). The total phenolic content was expressed as mg g^{-1}.

The contents of gallic acid, catechin, albiflorin, paeoniflorin, benzoic acid, and paeonol were determined by HPLC according to previously described protocols (Yu *et al.* 2006). HPLC system comprised of *Agilent 1260* liquid chromatography (*Agilent Technology Inc*., Santa Clara, CA, USA), *Waters* C18 column (4.6 mm × 250 mm, 5 μm). The test solution was filtered with a 0.22-μm organic membrane filter and detected using a gradient elution at 230 nm. The mobile phase consisted of a mixture of acetonitrile (A) and 0.05% phosphoric acid (pH 2.7, B). The gradient program was set as follows: 0 ~ 5 min, 8% ~ 12% A; 5 ~ 20 min, 12 ~ 20% A; 20 ~ 25 min, 20% A; 25 ~ 35 min, 20 ~ 45% A; 35 ~ 40 min, 45% A; 40 ~ 50 min, 45 ~ 8% A. The injection volume was 20 μL, the flow rate was set at 1.0 mL min^{-1}, and the column temperature was 30°C. The results were expressed as mg g^{-1}.

Statistical analysis: The measured data were analyzed by one-way analysis of variance (*ANOVA*) and *Duncan*'s test ($P<0.05$) with *SPSS 16.0* (*SPSS Inc*., Chicago, IL, USA). The measurement of biochemical parameters was determined by at least three biological repetitions.

Results

Effect of selenite on biochemical parameters: With the increase of selenite concentration, SOD activity, soluble protein, soluble sugar, and proline contents enhanced first and then decreased (Fig. 1). These four indexes in all selenite treatments were greatly higher than that in the control and reached the maximum value with the 30 mg L^{-1} selenite treatment.

REC of all selenite treatments was lower than that of the control (Fig. 1), with the lowest value and a significant difference under 30 mg(selenite) L^{-1}. MDA contents of all selenite treatments were significantly lower than that of the control, with the largest decrease in the 30 mg(selenite) L^{-1}. The contents of H_2O_2 and $O_2^{\bullet-}$ of 15–30 mg L^{-1} selenite treatments were significantly lower than those in the control, with a minimum value at the 30 mg(selenite) L^{-1}.

Pigment content and photosynthetic parameters: The contents of Chl *a*, Chl *b*, Car, and Chl (*a*+*b*) in all treatments showed a trend of rising first and then decreasing (Fig. 2). Chl *a* content of all selenite treatments was obviously higher than that of control. The changes in Chl *b* and Car content were similar, which were higher than the control in all selenite treatments, and markedly higher than the control only at the 30 mg(selenite) L^{-1}. The content of Chl (*a*+*b*) was significantly higher in all selenite treatments than that in the control. All pigment contents reached the maximum under the 30 mg L^{-1} selenite treatment.

The P_N under all selenite treatments was significantly higher than that of the control under 15–30 mg L^{-1} selenite

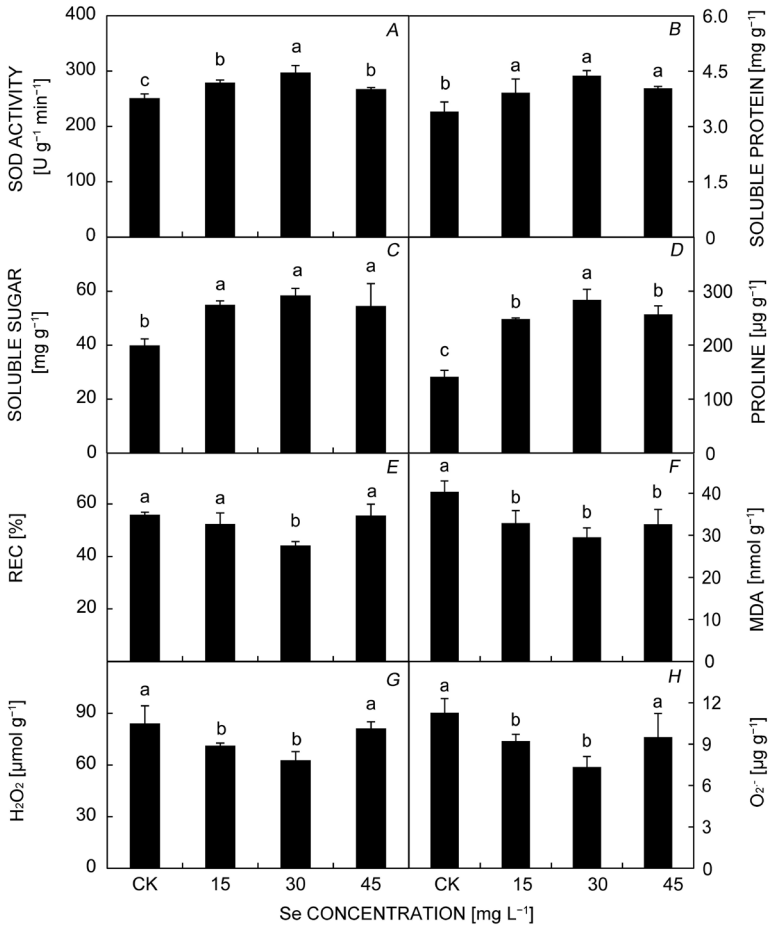

Fig. 1. Effect of different selenite treatments on the activity of SOD (*A*), and the content of soluble protein (*B*), soluble sugar (*C*), proline (*D*), REC (*E*), MDA (*F*), H_2O_2 (*G*), and $O_2^{\bullet-}$ (*H*) in *Paeonia ostii* leaves. Data represent the mean ± SD, $n = 3$. SOD – superoxide dismutase; MDA – malondialdehyde; REC – relative electrical conductivity. *Different lowercase letters* above the bars indicate a significant difference between treatments at $P<0.05$ as determined by a *Duncan*'s multiple range test.

treatment (Fig. 2). The change trends of g_s and E under different selenite treatments were similar, both increased significantly in all selenite treatments. Compared with the control group, the C_i of all selenite treatments increased, the increase was significant in 15 and 30 mg L^{-1} selenite treatments.

Effects of selenite on Chl fluorescence parameters: The F_v'/F_m', Φ_{PSII}, and ETR all increased first and then decreased with the increase of selenite concentration (Table 1). These three parameters all increased under all selenite treatments and reached the maximum value under the selenite treatment of 30 mg L^{-1}, which was significantly higher than the control.

Chl fluorescence OJIP curve and 820-nm modulation reflection curve: As shown in Fig. 3*A*, the K point (t = 0.3 ms) and J point (t = 2 ms) decreased in all selenite treatments, and the OJIP curve changed most obviously under 30 mg L^{-1} selenite treatment. The MR/MR_0 of the 820-nm reflection fluorescence absorption curve (Fig. 3*B*) in *P. ostii* decreased rapidly from 0.7 ms of JIP time to 3 ms linearly, and then slowly decreased to the minimum value between 3 and 30 ms. The minimum MR/MR_0 values of all selenite treatments decreased obviously, and 30 mg L^{-1} selenite treatment had the largest decrease, followed by 15 and 45 mg L^{-1} selenite treatments.

Fast Chl fluorescence parameters, the function and coordination of PSII and PSI of *P. ostii* leaves: The normalized fluorescence (W_K) of the K phase and the relative fluorescence change (V_J) of the J phase were calculated to quantify the changes of the K and J phase in the OJIP curve (Fig. 4). The values of W_K, V_J, and the initial slope of the relative variable fluorescence of the relative rate at which Q_A is reduced (M_0) decreased first and then increased, while the quantum yield for electron transport (φE_0) increased first and then decreased. The W_K and M_0 in all selenite treatments were significantly lower than those of the control (Fig. 4). In terms of V_J parameters, only V_J in 30 mg L^{-1} selenite treatment was significantly lower than that of the control. The φE_0 under 15–30 mg L^{-1} selenite treatment was significantly higher than that of the control, except for the 45 mg L^{-1} selenite treatment.

The parameters of the absorption flux per reaction center (ABS/RC), the dissipated energy flux per reaction center (DI_0/RC), the trapped energy flux per reaction center (TR_0/RC), and the electron transport flux per reaction center (ET_0/RC) decreased at first and then increased with the increase of selenite concentration (Table 1). The four parameters in all selenite treatments were significantly lower than those in the control, and the minimum values were all obtained in the 30 mg L^{-1} selenite treatment. The density of RCs per excited cross-section (RC/CS_m), the absorbed energy flux per cross-section (ABS/CS_m),

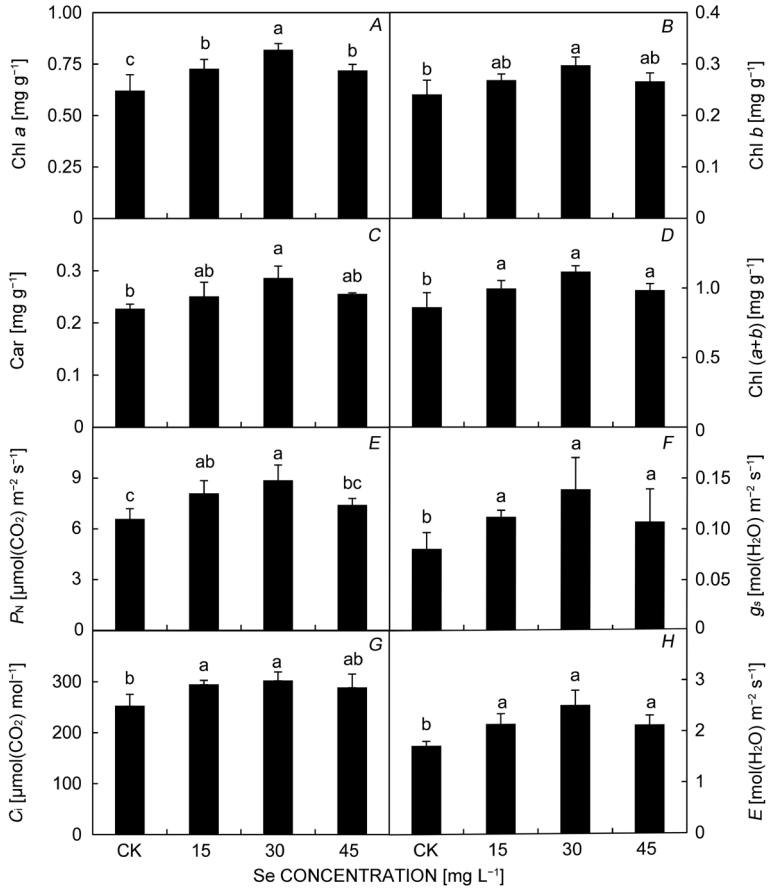

Fig. 2. Effect of different selenite treatments on the contents of Chl *a* (*A*), Chl *b* (*B*), Car (*C*), total Chl (*a*+*b*) (*D*), and P_N (*E*), g_s (*F*), C_i (*G*), *E* (*H*) in *Paeonia ostii* leaves. Chl – chlorophyll; Car – carotenoid; P_N – the net photosynthetic rate; g_s – stomatal conductance; C_i – intercellular carbon dioxide concentration; *E* – transpiration rate. Data represent the mean ± SD, $n = 3$ for leaf photosynthetic pigment concentrations, $n = 12$ for the photosynthetic parameters. *Different lowercase letters* above the bars indicate a significant difference between treatments at $P<0.05$ as determined by a *Duncan*'s multiple range test.

Table 1. The changes of the fluorescence parameters and the energy fluxes in *Paeonia ostii* leaves under different selenite treatments [mg L^{-1}]. F_v'/F_m' – the efficiency of excitation capture of open PSII center; Φ_{PSII} – the actual photochemical efficiency of PSII; ETR – the rate of electron transfer; ABS/RC – the absorption flux per reaction center; TR_0/RC – the trapped energy flux per reaction center; ET_0/RC – the electron transport flux per reaction center; DI_0/RC – the dissipated energy flux per reaction center; RC/CS_m – the density of RCs per excited cross-section; ABS/CS_m – the absorbed energy flux per cross-section; TR_0/CS_m – the trapped energy flux per cross-section; ET_0/CS_m – the electron transport flux per cross-section; DI_0/CS_m – the dissipated energy flux per cross-section; F_v/F_m – the maximum photochemical efficiency of PSII under dark adaptation; PI_{abs} – the performance index on absorption basis. Data represent the mean ± SD ($n = 12$). *Different lowercase letters* in each column indicate a significant difference between treatments at $P<0.05$ as determined by a *Duncan*'s multiple range test.

Parameters	0 (CK)	15	30	45
F_v'/F_m'	0.58 ± 0.04^{b}	0.61 ± 0.02^{b}	0.67 ± 0.01^{a}	0.60 ± 0.01^{b}
Φ_{PSII}	0.45 ± 0.03^{b}	0.48 ± 0.01^{b}	0.52 ± 0.01^{a}	0.47 ± 0.02^{b}
ETR	36.97 ± 2.50^{b}	39.13 ± 0.91^{b}	42.53 ± 0.93^{a}	39.07 ± 0.90^{b}
ABS/RC	1.42 ± 0.09^{a}	1.17 ± 0.03^{b}	1.03 ± 0.07^{c}	1.18 ± 0.03^{b}
DI_0/RC	0.43 ± 0.05^{a}	0.29 ± 0.02^{b}	0.26 ± 0.04^{b}	0.31 ± 0.02^{b}
TR_0/RC	1.02 ± 0.07^{a}	0.88 ± 0.02^{b}	0.78 ± 0.03^{c}	0.87 ± 0.05^{b}
ET_0/RC	0.58 ± 0.04^{a}	0.52 ± 0.02^{b}	0.50 ± 0.02^{b}	0.51 ± 0.01^{b}
RC/CS_m	$13{,}431.37 \pm 1{,}416.73^{c}$	$17{,}641.92 \pm 895.12^{b}$	$21{,}261.11 \pm 1{,}687.24^{a}$	$17{,}435.37 \pm 542.11^{b}$
ABS/CS_m	$23{,}803.00 \pm 666.18^{b}$	$24{,}728.75 \pm 796.92^{ab}$	$26{,}263.67 \pm 762.27^{a}$	$24{,}654.33 \pm 1{,}213.88^{ab}$
DI_0/CS_m	$7{,}251.00 \pm 151.92^{a}$	$6{,}173.50 \pm 233.26^{b}$	$6{,}326.33 \pm 590.53^{b}$	$6{,}245.00 \pm 209.82^{b}$
TR_0/CS_m	$16{,}985.33 \pm 641.74^{c}$	$18{,}805.25 \pm 645.88^{ab}$	$19{,}270.67 \pm 628.02^{a}$	$17{,}742.67 \pm 563.34^{bc}$
ET_0/CS_m	$10{,}446.00 \pm 392.74^{b}$	$11{,}234.75 \pm 683.91^{b}$	$12{,}433.33 \pm 537.67^{a}$	$11{,}045.67 \pm 397.05^{b}$
F_v/F_m	0.71 ± 0.02^{b}	0.75 ± 0.01^{a}	0.76 ± 0.02^{a}	0.74 ± 0.03^{ab}
PI_{abs}	2.35 ± 0.19^{c}	3.93 ± 0.72^{b}	5.43 ± 0.85^{a}	3.43 ± 0.28^{b}

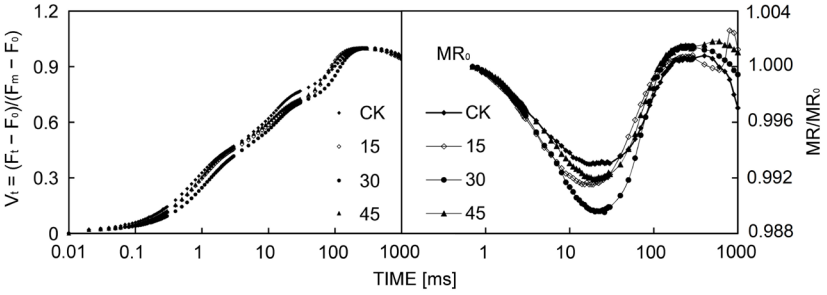

Fig. 3. The OJIP curve (*A*) and 820-nm reflection absorption curve (*B*) of tree peony under different selenite treatments. V_t – the relative variable fluorescence (V_t) at any time; O, K, J, I, and P – different phases in the OJIP curve. MR/MR_0 – the 820-nm modulated reflection curve; MR – the modulated reflection at different time points; MR_0 – the MR value of far-red light irradiated at 0.7 ms.

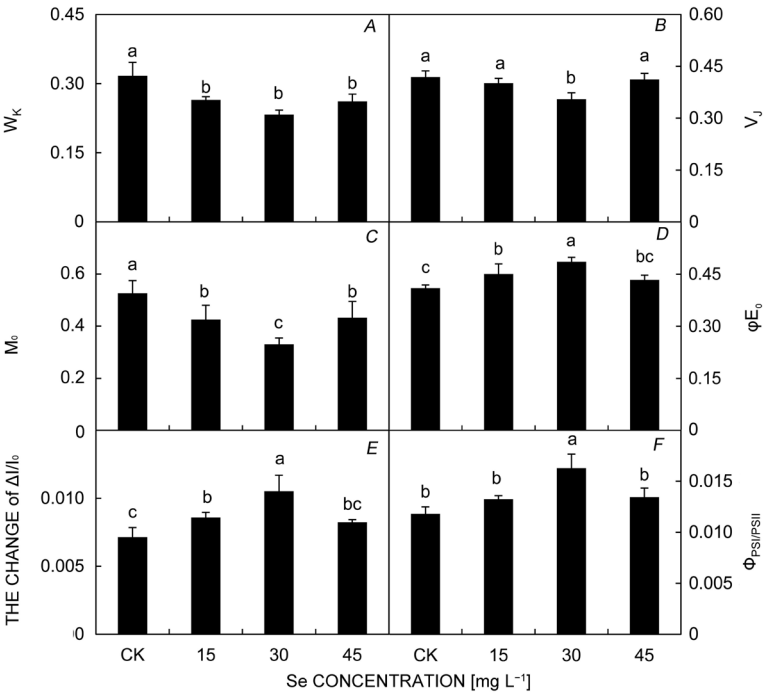

Fig. 4. The changes of W_K (*A*), V_J (*B*), M_0 (*C*), φE_0 (*D*), $\Delta I/I_0$ (*E*), and $\Phi_{PSI/PSII}$ (*F*) under different selenite treatments. W_K – the normalized relative variable fluorescence; V_J – the relative variable fluorescence intensity at the J step; M_0 – the initial slope of the relative variable fluorescence of the relative rate at which Q_A is reduced; φE_0 – the quantum yield for electron transport; $\Delta I/I_0$ – the maximum redox activity of PSI; $\Phi_{PSI/PSII}$ – the coordination between PSII and PSI. Data are means ± SD (n = 12). *Different lowercase letters* above the bars indicate a significant difference between treatments at $P<0.05$ as determined by a *Duncan*'s multiple range test.

the trapped energy flux per cross-section (TR_0/CS_m), the electron transport flux per cross-section (ET_0/CS_m), F_v/F_m, and the performance index on absorption basis (PI_{abs}) increased at first and then decreased with the increase of selenite concentration, reaching the maximum at 30 mg L^{-1} selenite treatment. The dissipated energy flux per cross-section (DI_0/CS_m) of all selenite treatments was significantly lower than those of the control.

$\Delta I/I_0$ and $\Phi_{PSI/PSII}$ increased in all selenite treatments (Fig. 4). The $\Delta I/I_0$ in 15 and 30 mg L^{-1} selenite treatments were greatly higher than those in the control, except for the 45 mg L^{-1} selenite treatment. The values of $\Phi_{PSI/PSII}$ of all selenite treatments increased more than those in the control but were only greatly higher than those of the control under the 30 mg L^{-1} selenite treatment. These two parameters all increased the most under the 30 mg L^{-1} selenite treatment.

Total flavonoids, total phenols, and secondary metabolites contents: With the increase of selenite application concentration, the contents of total flavonoids (Fig. 5*A*) and total phenols (Fig. 5*B*) in MCR were increased first and then decreased. The contents of total flavonoids and total phenols in all selenite treatments were higher than the control treatment, showing a significant difference in 15–30 mg L^{-1} selenite treatments. It is worth mentioning that the contents of total flavonoids and total polyphenols in the 30 mg L^{-1} selenite treatment increased more than those of other selenite treatments.

The changes in gallic acid (Fig. 5*C*) and paeonol (Fig. 5*H*) contents under different selenite treatments were similar, showing a trend of rising at first and then decreasing. These two parameters increased in all selenite treatments. The difference was that the content of gallic acid in the 30 mg L^{-1} selenite treatment was significantly higher than that in the control, while the content of paeonol in the 15–30 mg L^{-1} selenite treatments was significantly higher than that in the control. The change trend of catechin content (Fig. 5*D*) was similar to that of paeoniflorin content (Fig. 5*F*). The two parameters of all selenite treatments were significantly higher than those of the control, and those of 30–45 mg L^{-1} selenite treatments were significantly higher than those of other treatments, but there was no significant difference between the two treatments. The content of albiflorin (Fig. 5*E*) in all selenite treatments was significantly higher than that in the control, and the maximum increase was observed in 30–45 mg L^{-1} selenite treatments compared with the control group.

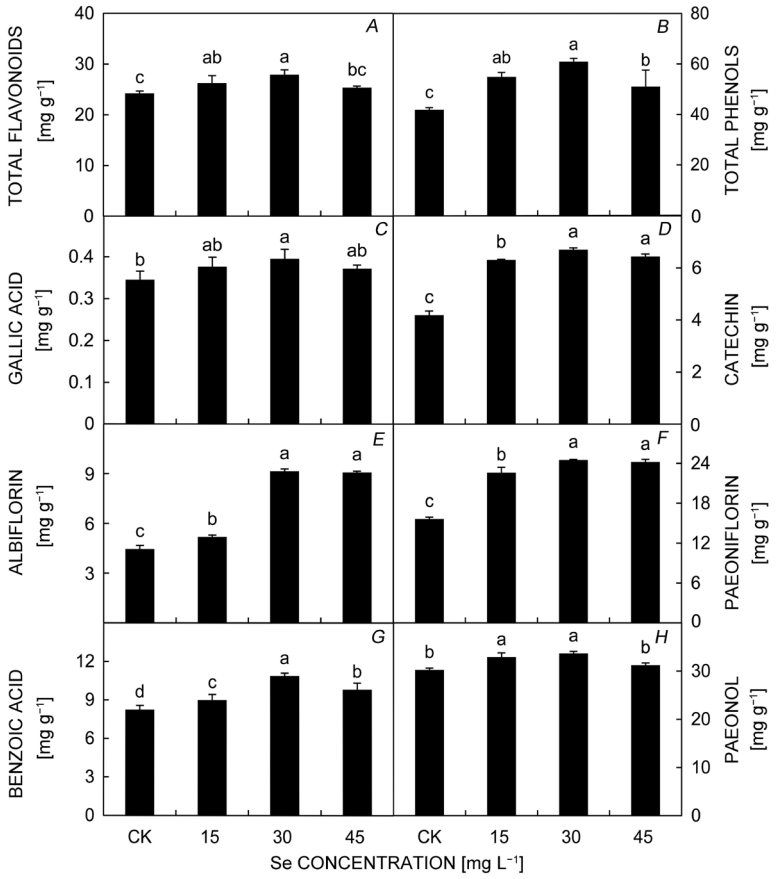

Fig. 5. Effect of different selenite treatments on the contents of total flavonoids (*A*), total polyphenols (*B*), gallic acid (*C*), catechin (*D*), albiflorin (*E*), paeoniflorin (*F*), benzoic acid (*G*), and paeonol (*H*) in MCR of *Paeonia ostii.* MCR – Moutan cortex radicis. Data are means ± SD (n = 3). *Different lowercase letters* above the bars indicate a significant difference between treatments at $P<0.05$ as determined by a *Duncan*'s multiple range test.

The content of benzoic acid (Fig. 5*G*) in all selenite treatments was significantly higher than that under the control, with the largest increase in the 30 mg L^{-1} selenite treatment.

Discussion

ROS, including H_2O_2 and $O_2^{\bullet-}$, are produced in different cellular metabolic pathways, which can cause oxidative stress and damage plant cells at high concentrations (Hasanuzzaman *et al*. 2021). In this study, the control treatment had higher contents of REC and MDA, indicating the presence of electrolyte leakage and membrane lipid peroxidation in the control plants due to photooxidation damage, which was also confirmed by the higher accumulation of H_2O_2 and $O_2^{\bullet-}$ in the control leaves.

Selenite can be metabolized into a series of organo-selenium compounds in plants, and organic derivatives of selenium, such as selenocysteine and selenomethylthione, can be used as antioxidants to react directly with ROS (Rahmanto and Davies 2012). In addition, selenium-containing proteins/peptides, in particular, have the powerful ability to neutralize free radicals such as $O_2^{\bullet-}$ and 2,2-biphenyl-1-picrylhydrazine (Zhu *et al*. 2019, Zhang *et al*. 2020). In this study, exogenous sodium selenite treatment obviously reduced the ROS content in *P. ostii*, which might be because sodium selenite application improved the synthesis of organic selenium compounds and selenium-containing proteins/peptides (Li *et al*. 2022b). On the other hand, previous studies have shown that selenite supplementation promoted the activities of enzymes such as GSH-Px, SOD, and POD (Chauhan *et al*. 2019). Consistent with previous studies, selenite pretreatment in this study increased SOD activity, which converts $O_2^{\bullet-}$ to H_2O_2, providing first-line protection against ROS. Studies have shown that plants can accumulate osmotic regulators such as soluble proteins and proline to regulate cell osmotic potential and stabilize cell structure (Varghese *et al*. 2019). Of note, soluble sugar and proline are also involved in the detoxification of ROS in different organelles (Malik *et al*. 2022). In this study, selenite treatment greatly increased the contents of soluble protein, soluble sugar and proline in *P. ostii*, maintained the osmotic potential in cells, and cooperated with antioxidant enzymes to remove ROS in cells, thus reducing membrane lipid peroxidation, as indicated by a significant decrease of REC, MDA, and H_2O_2 and $O_2^{\bullet-}$ contents in *P. ostii*. Similarly, the application of sodium selenite increased the SOD and POD activities, decreased MDA content, and increased soluble protein, chlorophyll, and proline contents in *Raphanus sativus* (Hu *et al.* 2022). Low concentrations of sodium selenite significantly increased the proline and total soluble sugar contents, as well as SOD, CAT, POD, APX, and glutathione reductase (GR), and decreased the MDA and H_2O_2 content in *Chenopodium quinoa* (Khalofah *et al.* 2021).

Appropriate selenite treatment increased the Chl content in *P. ostii* leaves, and similar results were also observed in

C. quinoa (Khalofah *et al*. 2021) and *R. sativus* (Hu *et al*. 2022). The increase in Chl content might occur because selenite application promoted the scavenging of ROS and protected Chl from photooxidation (Hawrylak-Nowak 2009). On the other hand, selenite application can increase the content of photosynthetic pigments by protecting chloroplast enzymes and promoting the biosynthesis of photosynthetic pigments (Chen *et al.* 2022).

In this study, the application of an appropriate amount of selenite induced an increase in P_N in *P. ostii* plants. As demonstrated in rice (Zhang *et al*. 2014), low concentrations of selenite had a positive effect on P_N, in support of our results. In this study, P_N, g_s, C_i, and E all increased after selenite treatments, suggesting that selenite could improve stomatal opening, which is conducive to CO_2 exchange and water transpiration, thus increasing the photosynthetic capacity of *P. ostii* leaves. The results of this study are similar to those in the other plants after selenite application (Zhang *et al*. 2014, de Almeida *et al*. 2022).

W_K reflects the injury of the oxygen-evolving complex (OEC) on the PSII donor side. V_J reflects the electron flow between quinone receptors Q_A and Q_B. M_0 represents the reduction rate of the primary quinone receptor (Q_A) and reflects the maximum closure rate of PSII reaction center. φE_0 is the quantum of light energy absorbed by the reaction center for electron transfer (Zhang *et al*. 2017). In this study, the application of selenite (30 mg L^{-1}) greatly increased the value of φE_0 and decreased V_J, indicating the improvement of the electron transfer ability of the PSI, which was confirmed by the increase in ETR. The significant decrease of the W_K and M_0 indicated that the application of selenite improved the function of OEC and integrity of the Mn_4CaO_5 complex, and decreased the maximum closing rate of the PSII reaction center (Souza *et al*. 2019, Guo *et al*. 2020). ROS is formed by the leakage of electrons attacking O_2 in the process of electron transport, and more ROS accumulation will damage the cell membrane and cause membrane peroxidation (Chalanika De Silva and Asaeda 2017). On the contrary, selenite treatment significantly improved the electron transport capacity in the photosystems, reduced electron leakage, decreased ROS contents, protected the stability of cell membrane and photosynthetic apparatus, and promoted the efficient operation of photosynthesis.

Compared with the control treatment, the ABS/RC, TR_0/RC, ET_0/RC, and DI_0/RC in selenite treatment (30 mg L^{-1}) were significantly reduced. The ABS/CS_m, TR_0/CS_m, and ET_0/CS_m of the selenite treatment were significantly higher than those of the control treatment, while the DI_0/CS_m was significantly lower than that of the control. In particular, selenite treatment significantly increased RC/CS_m of PSII. The above results indicated that selenite treatment could greatly reduce the energy charge pressure per reaction center of PSII by increasing the number of active reaction centers per cross-section (RC/CS_m) of PSII, improve the efficiency of energy conversion and utilization, and reduce the occurrence of photoinhibition (Chang *et al*. 2023).

F_v/F_m reflects the maximum photochemical efficiency of PSII under dark adaptation, F_v'/F_m' represents the maximum photochemical efficiency of PSII under light adaptation, Φ_{PSII} reflects the actual photochemical efficiency of PSII, and ETR represents the rate of electron transfer, PI_{abs} is the performance index of photosynthetic apparatus, which can comprehensively reflect the performance of PSII (Strasser *et al*. 2010). In this study, the significant increase of RC/CS_m, F_v/F_m, F_v'/F_m', Φ_{PSII}, ETR, and PI_{abs} of *P. ostii* showed that selenite treatment (30 mg L^{-1}) significantly improved the maximum photochemical efficiency of PSII, the light energy-utilization efficiency and the photosynthetic performance in PSII. Similar results were also observed in *Billbergia zebrina* (Souza *et al*. 2019) and *Medicago sativa* after Se treatment (Wang *et al*. 2022).

The redox activity of PSI is represented by 820-nm modulated reflectance curve, and MR/MR_0 reflects the ability of PSI reaction center to reduce terminal electron receptors (Yang *et al*. 2021). $\Delta I/I_0$ is used to comprehensively evaluate the performance of PSI, and $\Phi_{PSI/PSII}$ ($\Delta I/I_0/\psi_0$) represents the coordination between PSII and PSI (Zhang *et al*. 2021). In this study, the minimum value of MR/MR_0, $\Delta I/I_0$, and $\Phi_{PSI/PSII}$ decreased significantly after selenite treatment. These results showed that selenite treatment not only increased the activity of PSI reaction center, but also improved the mobility of electrons in both photosystems, thus significantly improving the coordination between PSII and PSI. Selenite treatment increased the content of photosynthetic pigments, the performance of PSII and PSI and the coordination between them, thus improving the photosynthetic capacity of leaves, which was also confirmed by the increase of P_N in *P. ostia*. In this study, selenite treatment increased photosynthesis, as well as soluble sugar and soluble protein content, finally provided sufficient carbohydrates for an increase in the total phenols and flavonoids and other substances.

Several studies showed phenols and flavonoid compounds can detoxify ROS, thereby protecting plant cells from photooxidation damage (Jucá *et al*. 2020, Wang *et al*. 2020b). In this study, the contents of total flavonoids, total phenols including gallic acid, catechins, and paeonol as well as benzoic acid, albiflorin and paeoniflorin were significantly increased by selenite treatment, which might contribute to scavenge ROS (Wang *et al.* 2017). Similar results were also reported in *Codonopsis lanceolata* (Zhu *et al.* 2017) and *B. juncea* (Li *et al.* 2023) after selenite treatment. In *C. lanceolata*, the contents of polysaccharides, total flavonoids, total saponins, proteins, total amino acids, and essential amino acids significantly increased at the level of the optimal selenium (Na_2SeO_3) treatment (1.0 mg L^{-1}), which significantly improved the nutritive quality of *C. lanceolata*, while 2.0 mg L^{-1} treatment reduced many nutritional indexes of *C. lanceolata* (Zhu *et al.* 2017). Application of selenium fertilizer (Na_2SeO_3) significantly increased the quality indexes of tomato fruits, such as total soluble solids, soluble sugar, titratable acid, sugar–acid ratio, vitamin C and lycopene, but had no significant effect on nitrate content and fruit hardness (Xu

et al. 2022). In this study, the 30 mg L^{-1} selenite treatment significantly increased the contents of total flavonoids, total phenols, and six medicinal components in MCR, while the content of total flavonoids, total phenols, benzoic acid, and paeonol at 45 mg L^{-1} of selenium showed a clear decrease. This suggests that the effect of selenium on quality improvement may vary depending on plant species, type of selenium fertilizer, concentration of Se, and method of fertilization.

Flavonoids are the largest group of phenolic compounds, and as other phenolic compounds are derived from phenylalanine (Balasundram *et al*. 2006). Studies have shown that selenite treatment of leaves induced the expression of key genes (*CHS* and *PAL*) in phenylpropionic acid metabolism in *Ginkgo biloba* leaves, and the transcription factors *MYB1* and *MYB2* involved in flavonoid biosynthesis were also significantly upregulated (Li *et al*. 2019). In *Arachis hypogaea*, selenite application upregulated the gene expression and related enzyme activities of the phenylpropanoid biosynthesis cascade, and finally increased the content of phenylpropanoid compounds including phenolic acid, lignin, and total flavonoids (Wang *et al*. 2016). In this study, the increase of flavonoids and phenols might be attributed to the upregulation of genes related to phenylpropionic acid metabolism induced by selenite treatment. Our results were consistent with previous studies on *C. lanceolata* (Zhu *et al*. 2017) and *Flammulina velutipes* (Dong *et al*. 2021) after sodium selenite application.

In the current study, selenite treatment also led to the enhancement of two monoterpenes constituents (paeoniflorin and albiflorin) in *P. ostii*. Recently, it has been found that selenite treatment can increase the content of monoterpenes (geranyl acetate, geranial, geraniol, nerol, and z-citral) (Azimi *et al*. 2021) and tetraterpenes (lycopene and β-carotene) (Morales-Espinoza *et al*. 2019) under non-stress conditions. Selenite treatment can affect transcription factors related to endogenous hormone regulation, and then regulate the expression of genes related to terpenoid synthesis, thereby promoting the accumulation of terpenoids, similar results were also found in *Ginkgo biloba* (Li *et al*. 2022a) treated with selenite.

Compared to soil application of selenium, foliar application is the most effective, safe, and economical method, and the efficiency of foliar application exceeds the efficiency of soil application by up to eight times (Poggi *et al*. 2000, Sattar *et al*. 2019). Xu *et al.* (2022) also found that Na_2SeO_3 had a more significant promoting effect on fruit quality variables than Na_2SeO_4 in tomato. Importantly, foliar application of selenite could greatly enhance the synthesis of organic selenium beneficial to humans and animals compared to selenate (Wang *et al*. 2020a). In this study, spraying sodium selenite significantly improved the antioxidant and photosynthetic capacity of medicinal *P. suffruticosa*, as well as the medicinal components in MCR, which has important application value in the cultivation of medicinal *P. suffruticosa*.

Conclusions: In this study, all selenite treatment had a positive effect on *P. ostii*, and the 30 mg L^{-1} selenite treatment was proved as the best. The 30 mg L^{-1} selenite treatment significantly increased the antioxidant capacity of *P. ostii* by increasing the activity of SOD enzymes and nonenzymatic active substances, such as carotenoids, soluble sugars, total polyphenols, and total flavonoids, greatly reduced the ROS contents, and enhanced the protection of photosynthetic apparatus. Moreover, selenite treatment significantly increased the pigment contents, enhanced the activity and coordination of PSII and PSI, greatly improved the photosynthetic capacity, and further increased the contents of paeonol, paeoniflorin, and other secondary metabolites. The results showed that selenite increased the content of medicinal components of *P. ostii* by improving the antioxidant system, osmotic adjustment substance content and photosynthetic capacity of *P. ostii*. This study provided important information for revealing the influence of exogenous selenite on the physiology and medicinal components accumulation of *P. ostii* and has important application value in the efficient cultivation of medicinal tree peony.

References

Ahmad Z., Anjum S., Skalicky M. *et al.*: Selenium alleviates the adverse effect of drought in oilseed crops camelina (*Camelina sativa* L.) and canola (*Brassica napus* L.). – Molecules **26**: 1699, 2021.

Alyemeni M.N., Ahanger M.A., Wijaya L. *et al.*: Selenium mitigates cadmium-induced oxidative stress in tomato (*Solanum lycopersicum* L.) plants by modulating chlorophyll fluorescence, osmolyte accumulation, and antioxidant system. – Protoplasma **255**: 459-469, 2018.

Azimi F., Oraei M., Gohari G. *et al.*: Chitosan-selenium nanoparticles (Cs–Se NPs) modulate the photosynthesis parameters, antioxidant enzymes activities and essential oils in *Dracocephalum moldavica* L. under cadmium toxicity stress. – Plant Physiol. Biochem. **167**: 257-268, 2021.

Balasundram N., Sundram K., Samman S.: Phenolic compounds in plants and agri-industrial by-products: Antioxidant activity, occurrence, and potential uses. – Food Chem. **99**: 191-203, 2006.

Bates L.S., Waldren R.P., Teare I.D.: Rapid determination of free proline for water-stress studies. – Plant Soil **39**: 205-207, 1973.

Cai H.L., Xie P.F., Zeng W.A. *et al.*: Root-specific expression of rice *OsHMA3* reduces shoot cadmium accumulation in transgenic tobacco. – Mol. Breeding **39**: 49, 2019.

Chalanika De Silva H.C., Asaeda T.: Effects of heat stress on growth, photosynthetic pigments, oxidative damage and competitive capacity of three submerged macrophytes. – J. Plant Interact. **12**: 228-236, 2017.

Chang Q.S., Zhang L.X., Chen S.C. *et al.*: Exogenous melatonin enhances the yield and secondary metabolite contents of *Prunella vulgaris* by modulating antioxidant system, root architecture and photosynthetic capacity. – Plants-Basel **12**: 1129, 2023.

Chauhan R., Awasthi S., Srivastava S. *et al.*: Understanding selenium metabolism in plants and its role as a beneficial element. – Crit. Rev. Env. Sci. Tec. **49**: 1937-1958, 2019.

Cheeseman J.M.: Hydrogen peroxide concentrations in leaves under natural conditions. – J. Exp. Bot. **57**: 2435-2444, 2006.

Chen H.U., Cheng Q., Chen Q.L. *et al.*: Effects of selenium on growth and selenium content distribution of virus-free sweet potato seedlings in water culture. – Front. Plant Sci. **13**:

965649, 2022.
Chen Y.H., Zhang X.R., Guo Q.S. *et al.*: Plant morphology, physiological characteristics, accumulation of secondary metabolites and antioxidant activities of *Prunella vulgaris* L. under UV solar exclusion. – Biol. Res. **52**: 17, 2019.
Cruz J.A., Avenson T.J.: Photosynthesis: A multiscopic view. – J. Plant Res. **134**: 665-682, 2021.
de Almeida H.J., Carmona V.V., Dutra A.F., Filho A.B.C.: Growth and physiological responses of cabbage cultivars biofortified with inorganic selenium fertilizers. – Sci. Hortic.-Amsterdam **302**: 111154, 2022.
Dong F., Wang C.Z., Sun X.D. *et al.*: Sugar metabolic changes in protein expression associated with different light quality combinations in tomato fruit. – Plant Growth Regul. **88**: 267-282, 2019.
Dong Z., Xiao Y., Wu H.: Selenium accumulation, speciation, and its effect on nutritive value of *Flammulina velutipes* (Golden needle mushroom). – Food Chem. **350**: 128667, 2021.
Feng S.M., Luo Z.S., Zhang Y.B. *et al.*: Phytochemical contents and antioxidant capacities of different parts of two sugarcane (*Saccharum officinarum* L.) cultivars. – Food Chem. **151**: 452-458, 2014.
Genty B., Briantais J.-M., Baker N.R.: The relationship between the quantum yield of photosynthetic electron transport and quenching of chlorophyll fluorescence. – BBA-Gen. Subjects **990**: 87-92, 1989.
Guo Y.Y., Li H.J., Liu J. *et al.*: Melatonin alleviates drought-induced damage of photosynthetic apparatus in maize seedlings. – Russ. J. Plant Physiol. **67**: 312-322, 2020.
Hasanuzzaman M., Raihan M.R.H., Masud A.A.C. *et al.*: Regulation of reactive oxygen species and antioxidant defense in plants under salinity. – Int. J. Mol. Sci. **22**: 9326, 2021.
Hawrylak-Nowak B.: Beneficial effects of exogenous selenium in cucumber seedlings subjected to salt stress. – Biol. Trace Elem. Res. **132**: 259-269, 2009.
Hu L., Wang X.L., Zou Y.T. *et al.*: Effects of inorganic and organic selenium intervention on resistance of radish to arsenic stress. – Ital. J. Food Sci. **34**: 44-58, 2022.
Jucá M.M., Cysne Filho F.M.S., de Almeida J.C. *et al.*: Flavonoids: biological activities and therapeutic potential. – Nat. Prod. Res. **34**: 692-705, 2020.
Kalaei M.H.R., Abdossi V., Danaee E.: Evaluation of foliar application of selenium and flowering stages on selected properties of Iranian Borage as a medicinal plant. – Sci. Rep.-UK **12**: 12568, 2022.
Kápolna E., Laursen K.H., Husted S., Larsen E.H.: Bio-fortification and isotopic labelling of Se metabolites in onions and carrots following foliar application of Se and ^{77}Se. – Food Chem. **133**: 650-657, 2012.
Khalofah A., Migdadi H., El-Harty E.: Antioxidant enzymatic activities and growth response of quinoa (*Chenopodium quinoa* Willd) to exogenous selenium application. – Plants-Basel **10**: 719, 2021.
Lanza M.G.D.B., Reis A.R.D.: Roles of selenium in mineral plant nutrition: ROS scavenging responses against abiotic stresses. – Plant Physiol. Biochem. **164**: 27-43, 2021.
Li L., Wu S., Wang S. *et al.*: Molecular mechanism of exogenous selenium affecting the nutritional quality, species and content of organic selenium in mustard. – Agronomy **13**: 1425, 2023.
Li L.L., Yu J., Li L. *et al.*: Treatment of *Ginkgo biloba* with exogenous sodium selenite affects its physiological growth, changes its phytohormones, and synthesizes its terpene lactones. – Molecules **27**: 7548, 2022a.
Li L.L., Yu J., Yuan H.H. *et al.*: High-Density kinetic analysis of the metabolomic and transcriptomic response of *Ginkgo biloba* flavonoids biosynthesis to selenium treatments. – Not. Bot. Horti. Agrobo. **47**: 792-803, 2019.
Li X.N., Brestic M., Tan D.X. *et al.*: Melatonin alleviates low PS I-limited carbon assimilation under elevated CO_2 and enhances the cold tolerance of offspring in chlorophyll *b*-deficient mutant wheat. – J. Pineal Res. **64**: e12453, 2018.
Li Y., Xiao Y., Hao J. *et al.*: Effects of selenate and selenite on selenium accumulation and speciation in lettuce. – Plant Physiol. Biochem. **192**: 162-171, 2022b.
Li Y.-T., Xu W.-W., Ren B.-Z. *et al.*: High temperature reduces photosynthesis in maize leaves by damaging chloroplast ultrastructure and photosystem II. – J. Agron. Crop Sci. **206**: 548-564, 2020.
Lichtenthaler H.K.: Chlorophyll and carotenoids: Pigments of photosynthetic biomembranes. – Method. Enzymol. **148**: 350-382, 1987.
Liu L., Wang L.X., Lv L.H. *et al.*: Improvement of growth and quality and regulation of the antioxidant system and lipid peroxidation in Chinese cabbage (*Brassica pekinensis* (Lour.) Rupr.) by exogenous sodium selenite. – Appl. Ecol. Env. Res. **18**: 7473-7481, 2020.
Longchamp M., Castrec-Rouelle M., Biron P., Bariac T.: Variations in the accumulation, localization and rate of metabolization of selenium in mature *Zea mays* plants supplied with selenite or selenate. – Food Chem. **182**: 128-135, 2015.
Malagoli M., Schiavon M., dall'Acqua S., Pilon-Smits E.A.H.: Effects of selenium biofortification on crop nutritional quality. – Front. Plant Sci. **6**: 280, 2015.
Malik Z., Afzal S., Dawood M. *et al.*: Exogenous melatonin mitigates chromium toxicity in maize seedlings by modulating antioxidant system and suppresses chromium uptake and oxidative stress. – Environ. Geochem. Hlth. **44**: 1451-1469, 2022.
Morales-Espinoza M.C., Cadenas-Pliego G., Pérez-Alvarez M. *et al.*: Se nanoparticles induce changes in the growth, antioxidant responses, and fruit quality of tomato developed under NaCl stress. – Molecules **24**: 3030, 2019.
Poggi V., Arcioni A., Filippini P., Pifferi P.G.: Foliar application of selenite and selenate to potato (*Solanum tuberosum*): Effect of a ligand agent on selenium content of tubers. – J. Agr. Food Chem. **48**: 4749-4751, 2000.
Puccinelli M., Pezzarossa B., Rosellini I., Malorgio F.: Selenium enrichment enhances the quality and shelf life of basil leaves. – Plants-Basel **9**: 801, 2020.
Rahmanto A.S., Davies M.J.: Selenium-containing amino acids as direct and indirect antioxidants. – IUBMB Life **64**: 863-871, 2012.
Rider S.A., Davies S.J., Jha A.N. *et al.*: Bioavailability of co-supplemented organic and inorganic zinc and selenium sources in a white fishmeal-based rainbow trout (*Oncorhynchus mykiss*) diet. – J. Anim. Physiol. Anim. Nutr. **94**: 99-110, 2010.
Sattar A., Cheema M.A., Sher A. *et al.*: Physiological and biochemical attributes of bread wheat (*Triticum aestivum* L.) seedlings are influenced by foliar application of silicon and selenium under water deficit. – Acta Physiol. Plant. **41**: 146, 2019.
Souza A.F.C., Martins J.P.R., Gontijo A.B.P.L., Falqueto A.R.: Selenium improves the transport dynamics and energy conservation of the photosynthetic apparatus of *in vitro* grown *Billbergia zebrina* (Bromeliaceae). – Photosynthetica **57**: 931-941, 2019.
Strasser R.J., Tsimilli-Michael M., Qiang S., Goltsev V.: Simultaneous *in vivo* recording of prompt and delayed fluorescence and 820-nm reflection changes during drying and after rehydration of the resurrection plant *Haberlea*

rhodopensis. – BBA-Bioenergetics **1797**: 1313-1326, 2010.
Sun J., Chen T., Liu M. *et al.*: Analysis and functional verification of *PoWRI1* gene associated with oil accumulation process in *Paeonia ostii*. – Int. J. Mol. Sci. **22**: 6996, 2021.
Varghese N., Alyammahi O., Nasreddine S. *et al.*: Melatonin positively influences the photosynthetic machinery and antioxidant system of *Avena sativa* during salinity stress. – Plants-Basel **8**: 610, 2019.
Wang G., Wu L.Y., Zhang H. *et al.*: Regulation of the phenylpropanoid pathway: A mechanism of selenium tolerance in peanut (*Arachis hypogaea* L.) seedlings. – J. Agr. Food Chem. **64**: 3626-3635, 2016.
Wang H., Cui X.X., Zhao X.G. *et al.*: Differences of biochemical constituents and contents of eight cultivars flowers of *Camellia sinensis*. – J. Essent. Oil Bear. Pl. **18**: 320-328, 2015.
Wang M., Ali F., Wang M. *et al.*: Understanding boosting selenium accumulation in wheat (*Triticum aestivum* L.) following foliar selenium application at different stages, forms, and doses. – Environ. Sci. Pollut. R. **27**: 717-728, 2020a.
Wang Q.D., Hu J.K., Hu H.F. *et al.*: Integrated eco-physiological, biochemical, and molecular biological analyses of selenium fortification mechanism in alfalfa. – Planta **256**: 114, 2022.
Wang Z.Q., He C.N., Peng Y. *et al.*: Origins, phytochemistry, pharmacology, analytical methods and safety of cortex moutan (*Paeonia suffruticosa* Andrew): a systematic review. – Molecules **22**: 946, 2017.
Wang Z.Q., Zhu C.J., Liu S.S. *et al.*: Comprehensive metabolic profile analysis of the root bark of different species of tree peonies (*Paeonia* Sect. Moutan). – Phytochemistry **163**: 118-125, 2019.
Wang Z.Y., Li S.Y., Ge S.H., Lin S.L.: Review of distribution, extraction methods, and health benefits of bound phenolics in food plants. – J. Agr. Food Chem. **68**: 3330-3343, 2020b.
Xu X., Wang J., Wu H. *et al.*: Effects of selenium fertilizer application and tomato varieties on tomato fruit quality: A meta-analysis. – Sci. Hortic.-Amsterdam **304**: 111242, 2022.
Yang H., Zhang J.T., Zhang H.W. *et al.*: Effect of 5-aminolevulinic acid (5-ALA) on leaf chlorophyll fast fluorescence characteristics and mineral element content of *Buxus megistophylla* grown along urban roadsides. – Horticulturae **7**: 95, 2021.
Yu K., Wang Y.W., Cheng Y.Y.: Determination of the active components in Chinese herb cortex moutan by MEKC and LC. – Chromatographia **63**: 359-364, 2006.
Zhang L.X., Chang Q.S., Hou X.G. *et al.*: Biochemical and photosystem characteristics of wild-type and Chl *b*-deficient mutant in tree peony (*Paeonia suffruticosa*). – Photosynthetica **59**: 256-265, 2021.
Zhang L.X., Chang Q.S., Hou X.G. *et al.*: The effect of high temperature stress on the physiological indexes, chloroplast ultrastructure, photosystems of two herbaceous peony cultivars. – J. Plant Growth Regul. **42**: 1631-1646, 2023.
Zhang M., Tang S.H., Huang X. *et al.*: Selenium uptake, dynamic changes in selenium content and its influence on photosynthesis and chlorophyll fluorescence in rice (*Oryza sativa* L.). – Environ. Exp. Bot. **107**: 39-45, 2014.
Zhang X., He H., Xiang J.Q. *et al.*: Selenium-containing proteins/peptides from plants: A review on the structures and functions. – J. Agr. Food Chem. **68**: 15061-15073, 2020.
Zhang Z.S., Liu M.J., Scheibe R. *et al.*: Contribution of the alternative respiratory pathway to PSII photoprotection in C_3 and C_4 plants. – Mol. Plant **10**: 131-142, 2017.
Zhu L.X., Wang P., Zhang W.J. *et al.*: Effects of selenium application on nutrient uptake and nutritional quality of *Codonopsis lanceolata*. – Sci. Hortic.-Amsterdam **225**: 574-580, 2017.
Zhu S., Du C.D., Yu T. *et al.*: Antioxidant activity of selenium-enriched peptides from the protein hydrolysate of *Cardamine violifolia*. – J. Food Sci. **84**: 3504-3511, 2019.

Appendix 1. JIP parameters analysis.

Fluorescence parameters	Description
$W_K = (F_K – F_0)/(F_J – F_0)$	Normalized relative variable fluorescence
$V_J = (F_J – F_0)/(F_m – F_0)$	Relative variable fluorescence intensity at the J step
$M_0 = 4(F_{300\mu s} – F_0)/(F_m – F_0)$	Initial slope of the relative variable fluorescence of the relative rate at which Q_A is reduced
$\varphi E_0 = ET_0/ABS = [1– (F_0/F_m)]\psi_0$	Quantum yield for electron transport
$ABS/RC = M_0(1/V_J)(1/\varphi P_0)$	Absorption flux per reaction center
$TR_0/RC = M_0(1/V_J)$	Trapped energy flux per reaction center
$ET_0/RC = M_0(1/V_J)\psi E_0$	Electron transport flux per reaction center
$DI_0/RC = (ABS/RC) – (TR_0/RC)$	Dissipated energy flux per reaction center
$RC/CS_m = \varphi P_0(V_J/M_0)(ABS/CS_m)$	Density of RCs per excited cross-section
$ABS/CS_m \approx F_m$	Absorbed energy flux per cross-section
$TR_0/CS_m = \varphi P_0(ABS/CS_m)$	Trapped energy flux per cross-section
$ET_0/CS_m = \varphi E_0(ABS/CS_m)$	Electron transport flux per cross-section
$DI_0/CS_m = ABS/CS_m – TR_0/CS_m$	Dissipated energy flux per cross-section
F_v'/F_m'	Efficiency of excitation capture of open PSII center
F_v/F_m	Maximal quantum yield of PSII photochemistry
$PI_{abs} = (RC/ABS)[\varphi P_0/(1 – \varphi P_0)][\psi_0/(1 – \psi_0)]$	Performance index on absorption basis